Estimating the Indistinguishability of Heralded Single Photons Using Second-Order Correlation

Imad I. Faruque[1,*] Gary F. Sinclair,[1] Damien Bonneau,[1] Takafumi Ono,[1,2,3] Christine Silberhorn,[4] Mark G. Thompson,[1] and John G. Rarity[1]

[1]*Quantum Engineering Technology Laboratory, University of Bristol, Bristol BS8 1TL, United Kingdom*

[2]*PRESTO, Japan Science and Technology Agency (JST), Kawaguchi, Saitama 332-0012, Japan*

[3]*National Institute of Information and Communications Technology (NICT), 4-2-1 Nukui-Kitamachi, Koganei, Tokyo 184-8795, Japan*

[4]*Applied Physics, University of Paderborn, Warburger Strasse 100, 33098 Paderborn, Germany*

Integrated quantum photonics is a promising strand of research that involves guiding light in submicron-scale structures and utilizing the quantum properties of the fundamental particle of light—the photon. One of these quantum properties, the indistinguishability of the photons, is used to achieve high-visibility quantum interference, which is one of the key resources in photonic quantum information processing. Here, we demonstrate that the faster and simpler heralded and unheralded second-order correlation functions ($g^{(2)}$) estimate the visibility (indistinguishability) well without the need to perform laborious and time-consuming quantum-interference measurements.

I. INTRODUCTION

It has long been known that if two completely identical single photons meet at a 50:50 beam splitter, they bunch and leave the beam splitter together. This counterintuitive quantum effect has come to be known as Hong-Ou-Mandel (HOM) interference, after the authors who have demonstrated it [1]. More recently, the importance of high-visibility HOM interference has been highlighted as the key to making high-fidelity linear-optics quantum gates [2–4] that are essential in order to realize scalable routes to quantum computation [5–7], which might require many millions of gates. In recent years, relatively complex quantum-photonic circuits have been made, demonstrating quantum-information tasks such as multidimensional quantum entanglement [8], arbitrary two-qubit processing [9], faster boson sampling [10,11], and graph state generation [12], all of which rely on high-visibility interference between photons from independent single-photon sources (SPSs). Among these examples, silicon-on-insulator (SOI) quantum photonics stands out due to its complex architecture [13], small device footprints, fast switches [14], electronic integration [15], and advances toward midscale integration. The presently achievable interference visibilities limit the fidelity of these circuits and prove a key bottleneck to achieving large-scale quantum information processors.

Experiments using bulk-optics parametric photon-pair (i.e., signal and idler) sources can reach >99% interference visibility [16] when the photons are fully entangled in energy and time at the point of creation. However, scalability beyond two photons requires interference of photons from separated sources where no entanglement pre-exists. In this case, several factors can reduce the interference visibility. The first is the need for photons to be in a single mode both spatially and spectrotemporally. Creating photons in single-mode waveguide devices solves spatial-mode overlap problems, especially in SOI photonics, which is mature and has high fabrication precision, as we do not observe any discernible spatial distinguishability [17]. Spectrotemporal overlap is usually ensured by pumping with a pulsed laser, which then leads in the spectral domain to a broadened energy-conservation constraint, resulting in a joint spectrum that shows weaker correlations between the photon pairs. These undesired spectral correlations make it possible to distinguish the heralded photon energy by measuring the idler photon, which would result in a decreased heralded-photon purity. However, this correlation can be removed by careful engineering of phase matching [18,19], by cavity schemes [20,21], or simply by filtering both the signal and the idler beams to bandwidths narrower than the pump [22–25]. The single-mode nature or purity of the joint spectrum can then be analyzed by decomposing into orthogonal modes

_____
*imad.faruque@bristol.ac.uk

and estimating the contribution of higher modes [26]. The second problem is that the emission of photon pairs in the parametric process is probabilistic, showing (identical) thermal statistics in each generated photon beam. Heralding with standard detectors only determines that there is a minimum of one photon heralded and higher-order emissions then contribute to a background coincidence rate after the beam splitter, thus reducing the visibility. These two processes are defined as the spectral purity and the photon-number purity of our heralded single-photon sources (HSPSs).

By measuring the heralded-HOM interference visibility, we directly measure the combined effects of spectral and number purity, which can be corrected for background coincidences [24] to assess the spectral indistinguishability. This is a fourfold coincidence experiment in which the count rates are extremely low. However, it has been implicit since the groundbreaking experiments of Hanbury Brown and Twiss [27] that two-intensity (i.e., two-photon) interference is intrinsic to thermal light. The decay from 2 to 1 of the second-order intensity correlation function [$g^{(2)}(0)$] reflects the fact that photons are in separate temporal or spatial modes [28]. It has then been noted that this provides a simple and rapid measure of the degree of purity of SPSs [29]. A few experimental works have used this technique to estimate the spectral purity [30–34] but the purity estimated in these works was not rigorously compared with the visibility of the quantum interference, the purity estimated from joint-spectral-intensity (JSI), or theoretical predictions, thus leaving questions as to the reliability of this technique. In addition, the validity of this method in the presence of noise is scarcely discussed [35]. In this paper, we show experimentally that the $g^{(2)}(0)$ method gives equivalent results to HOM dip visibilities taking into account both photon-number and spectral-purity effects.

In this paper, we perform both heralded and unheralded $g^{(2)}$ experiments, compare these with quantum-interference experiments, and discuss the results in terms of both photon-number purity and spectral purity. We also measure the pump phase profile using a frequency-resolved optical gating (FROG) and use this in the simulations, leading to improved agreement with the experiment. We find that the $g^{(2)}$ measurements are more straightforward and faster to measure the spectral purity and thus to infer the indistinguishability of well-fabricated silicon strip-waveguide HSPSs, without actually performing the more laborious and time-consuming quantum-interference experiments, which become exponentially demanding for measuring pairwise indistinguishability among multiple on-chip SPSs. Although, for our experiments, we use SOI strip-waveguide sources with external filtering to provide indistinguishability, the method applies to most other integrated guided-wave spontaneous pair-generation sources.

II. SILICON STRIP WAVEGUIDE AS AN HSPS

The $\chi^{(3)}$ nonlinearity in silicon gives rise to a spontaneous four-wave mixing (SFWM) process that generates correlated photon pairs. In SFWM, two pump photons (ω_p) interact with the vacuum field and transform into a pair of photons, historically called a signal and an idler (ω_s, ω_i), with different wavelengths. The energy and momentum of this process is conserved and is governed by the input-pump profile, the material properties, the geometry of the waveguide structure, and the mode profile. These factors ultimately determine the degree of correlation of the generated photons and therefore the spectral purity. If the frequency of the pump and signal-idler photons are expressed by ω_p, ω_s, and ω_i and the momentum by $\vec{k}_p$, $\vec{k}_s$, and $\vec{k}_i$, then the energy and momentum conservation of the SFWM process can be written in general as follows [36]:

$$2\hbar\omega_p = \hbar\omega_s + \hbar\omega_i, \tag{1}$$

$$2\vec{k}_p = \vec{k}_s + \vec{k}_i. \tag{2}$$

Quantum mechanically, the interactions among the pump beam and the signal-idler photon pairs can be described by an effective Hamiltonian $\hat{H}$ [37] and the generated photon pairs by a wave function $|\Psi\rangle$:

$$\hat{H} = N \int \int d\omega_s d\omega_i f(\omega_s, \omega_i) \, \hat{a}^\dagger(\omega_s) \, \hat{a}^\dagger(\omega_i) + \text{H.c.}, \tag{3}$$

$$|\Psi\rangle = \exp\left(\frac{-i}{\hbar}\hat{H}\right) |0, 0\rangle, \tag{4}$$

where the normalization constant N is related to the strength of the interaction, H.c. represents the Hermitian conjugate, $\hat{a}^\dagger(\omega_s)$, $\hat{a}^\dagger(\omega_i)$ represent creation operators of the signal and idler photons, respectively, and the biphoton function or joint spectral density (JSD) $f(\omega_s, \omega_i)$ contains the energy and momentum conservation of the interaction:

$$f(\omega_s, \omega_i) = \int d\omega_p \alpha(\omega_p)\alpha(\omega_s + \omega_i - \omega_p)\phi(\omega_p, \omega_s, \omega_i) \tag{5}$$

$$= f_A(\omega_s, \omega_i) \, \exp\left[-if_P(\omega_s, \omega_i)\right] \tag{6}$$

$$= \sum_{k=1}^{\infty} \lambda_k h_k(\omega_s) \times g_k(\omega_i), \tag{7}$$

where $\alpha(\omega)$ and $\phi(\omega_p, \omega_s, \omega_i)$ represent the pump spectral distribution and the phase-matching condition, respectively. The amplitude and phase of the JSD are called the joint spectral amplitude (JSA) and the joint spectral phase (JSP), denoted by f_A and f_P, respectively. In the last line, Schmidt decomposition [26] is used to express the JSD

in terms of orthogonal and separable signal-idler functions (h_k, g_k).

Spectral purity (P) is then quantified by tracing the square of the density matrix of the heralded signal photon, $\hat{\rho}_s$:

$$\hat{\rho}_s = \text{tr}_i(|\Psi\rangle\langle\Psi|), \tag{8}$$

$$P = \text{tr}(\hat{\rho}_s^2) = \sum \lambda_k^4. \tag{9}$$

If there is no frequency correlation between the signal-idler photons, then the heralded photons will be projected into one single optical mode ($k = 1$) and the spectral purity will be unity ($\rho_s^2 = \rho_s$).

Spectral filtering is a method of improving the spectral purity as it modifies the JSD and consequently reduces the frequency correlation. Mathematically, the effect of filtering on the JSD is expressed as follows:

$$f(\omega_s, \omega_i) = \int d\omega_p \alpha(\omega_p)\alpha(\omega_s + \omega_i - \omega_p)\phi(\omega_p, \omega_s, \omega_i)F_p(\omega_p)F_p(\omega_s + \omega_i - \omega_p)F_s(\omega_s)F_i(\omega_i), \tag{10}$$

where F represents the spectral filters. During the JSD calculation for unheralded $g^{(2)}(0)$, F_i is omitted in the above equation.

From the above discussions, it is evident that the pump phase profile plays a significant role in the separability of the JSP (f_P). If the pump phase profile is flat (constant phase), then from Eqs. (5) and (10) we can see that the JSP is factorable. A varying pump phase profile can thus further reduce the purity significantly. One way to measure the spectral purity is to reconstruct the JSA by using a single-photon spectrometer. This method requires very bright HSPSs; the resolution is low and does not measure the JSP. Recently, stimulated emission tomography has become popular for the measurement of both the JSA and the JSP [38,39]. The JSP correlation of a photon pair from the HSPSs has been investigated previously [40], but not in the context of spectral purity and excluding the effect of the pump phase profile.

A comparatively simpler method (and one that includes the whole JSD) for the spectral-purity measurement is the unheralded second-order correlation function $g^{(2)}(0)$, which is implemented by using a Hanbury Brown and Twiss (HBT) interferometer [27]. If the signal photons are spectrally pure, then the unheralded $g^{(2)}(0)$ approaches a value of 2, mimicking thermal statistics. If they are spectrally very impure, then the $g^{(2)}(0)$ value approaches 1, mimicking Poissonian statistics of a coherent state. When the squeezing is low, the spectral purity

and the $g^{(2)}(0)$ values are related by the following equation [29]:

$$g^{(2)}(0) = 1 + P. \tag{11}$$

It is known that in the absence of the higher photon-number terms—i.e., in the low-brightness limit (see, e.g., Ref. [22])—the visibility (V) of the HOM interference between two identical HSPSs (e.g., A and B) represents the spectral purity, $V = P$ (see the Supplemental Material [41]). However, in general, the visibility will depend on the brightness of each individual Schmidt mode in a nontrivial way. We find an expression for the visibility:

$$V = \frac{\sum_{p=0}^{\infty}\left[P_{4f}^{\text{dist}}(\mu_p^A, \mu_p^B) - P_{4f}^{\text{ind}}(\mu_p^A, \mu_p^B)\right]}{\sum_{p,q=0}^{\infty}P_{4f}^{\text{dist}}(\mu_p^A, \mu_q^B)}, \tag{12}$$

where P_{4f}^{dist}, P_{4f}^{ind} are the probabilities of fourfold events in the HOM interference for completely distinguishable and indistinguishable photons, respectively; μ_p^A, μ_p^B are mean photon numbers from HSPSs A and B, respectively; and the sums in p and q are over each Schmidt mode. The derivation of this equation is in the Supplemental Material [41] and is based on earlier work on the spectral decomposition of two-mode squeezed states [42], with the inclusion of higher-order photon-number terms [25].

Experimentally, the HOM visibility (i.e., indistinguishability) of a silicon strip-waveguide HSPS has been demonstrated to reach 72% [25] and then 88% [43] by using successively narrower spectral filtering (filter and pump widths not specified) with a reduced pump power (i.e., a higher photon-number purity). Therefore, the multimodal effect (i.e., the spectral purity) and the multipair effect (i.e., the photon-number purity) need to be addressed together to estimate the visibility of the quantum interference correctly.

In this paper, we perform two sets of experiments. The first uses heralded and unheralded $g^{(2)}(0)$ experiments to measure the spectral and photon-number purity. The spectral purity is quantified as a function of the spectral filtering and the photon-number purity is quantified as a function of the pump power. In the second set of experiments, the HOM interference is used to measure the raw indistinguishability as a function of both the spectral purity and the photon-number purity. The data are available in Ref. [44].
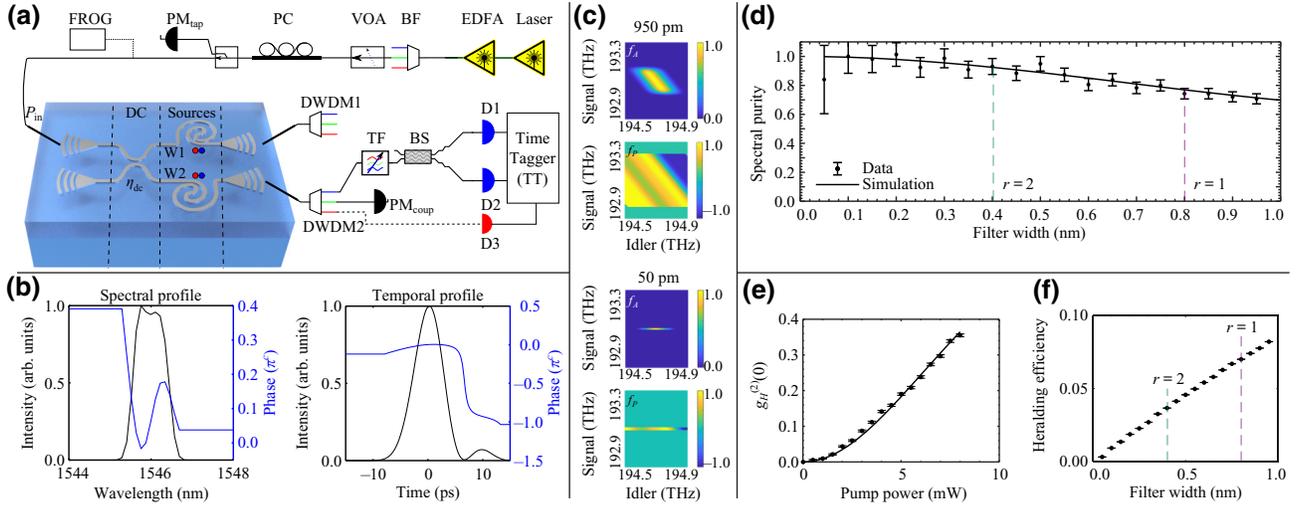
FIG. 1. The $g^{(2)}(0)$ measurements contain both the spectral purity and the photon-number purity: (a) the experimental setup; (b) the pump-pulse amplitude and phase profile from FROG measurements; (c) the JSD simulations; (d) the spectral purity as a function of the spectral filtering; (e) the heralded $g_H^{(2)}(0)$ as a function of the input power—the photon-number purity $= 1 - g_H^{(2)}(0)$; (f) the raw heralding efficiency as a function of the filtering. PM: power meter; PC: polarisation controller; VOA: variable optical attenuator; BF: bandpass filter; DC: directional coupler; W1: waveguide 1; W2: waveguide 2; η_{dc}: represents the splitting ratio of the coupler.

III. SECOND-ORDER CORRELATION [$g^{(2)}(0)$] MEASUREMENTS

The purities of the single photons are measured by using the second-order correlation function $g^{(2)}(0)$ as shown in Fig. 1(a). A pulsed laser (PriTel FFL) of 50-MHz repetition rate is first cleaned with broadband filters by attenuating the pump intensity by about 120 dB in the signal-idler collection spectra. It is then coupled to the silicon-photonic chip using a vertical-grating coupler (VGC) with a 4.5-dB loss at the best coupling. In the chip, a directional coupler splits the power for the two strip waveguides of length 14 mm. While the light propagates in the waveguide, the nonlinear optical process SFWM coherently generates signal-idler photon pairs. At the end of one of the waveguides, they are coupled out using another VGC. Afterward, a dense-wavelength-division-multiplexer (DWDM) filter separates the signal and idler photons. The signal photons then pass through a tunable bandwidth filter (TF). The output of the TF is connected to an HBT interferometer to measure the spectral purity of the signal photons. In the HBT interferometer, the signal photons are input into the port of an even beam splitter and the two outputs are connected to two superconducting single-photon detectors (SSPDs), D1 and D2, which are connected to the time tagger (TT). TT implements the time delay (τ) in $g^{(2)}(\tau)$ electronically to normalize $g^{(2)}(0)$. The idler photons may or may not be detected (D3), leading to two different configurations as shown by the dotted line in Fig. 1(a). In the first configuration, they are not detected and therefore do not project the signal photons into specific spectrotemporal

modes, thereby measuring the spectral purity of the signal photons through unheralded $g^{(2)}(0)$. In the second configuration, when all three of the detectors are used, it is then called a heralded second-order correlation measurement $g_H^{(2)}(0)$, which measures the photon-number purity of the HSPS. This configuration is also used to measure the heralding efficiency, where the counts from the two output ports of the BS are added together. These two configurations investigate the trade-off between the heralding efficiency and the spectral purity and measure the photon-number purity.

In both configurations, an approximately 0.8-nm-width pump pulse is chosen. Using a commercial FROG, the spectrogram of the pump pulse is measured to reconstruct the amplitude and phase profiles, as shown in Fig. 1(b). The pump phase profile is not flat as assumed by most quantum-photonic experiments. In fact, there is a slight variation of the phase on the central wavelength in comparison to the tail end of the pulse, with values between 0.2π and 0.4π. These amplitude and phase profiles are used in conjunction with linear interpolation to compute the JSDs (and thus the purity) using Eq. (10) as a function of the spectral filtering. Figure 1(c) shows the computed JSDs (JSAs and JSPs) for the broadest (950 pm) and narrowest (50 pm) filtering configuration of the TF. For the broader filter setting, the correlation between the signal and idler photons reduces the spectral purity to $P = 71.39\%$. For a constant phase profile, as assumed in most quantum-photonic experiments, the spectral purity is computed as $P = 72.27\%$, which is 0.8% above the value obtained with a varying pump phase profile. At the narrowest filter

setting, the JSD becomes almost a horizontal line, thereby removing the frequency correlation as the spectral purity approaches unity ($P \approx 1$).

The simulated purity (black line) and the estimated purity (black dots) from the $g^{(2)}(0)$ measurement (without any background corrections) are plotted in Fig. 1(d), showing the general trend that filtering improves purity. If the measured phase profile is included, then the graph moves downward (lower P) much more for broader TF filters. For example, the purity decreases by about 0.8% when TF is 950 pm compared to about 0.1% for when TF is 200 pm. The purity is essentially determined by the ratio (r) of the pump line width (Δ_{pump}) to the signal-idler filter line width (Δ_{signal}),

$$r = \frac{\Delta_{pump}}{\Delta_{signal}} \qquad (13)$$

Figure 1(f) shows that the measured heralding efficiency decreases with narrower spectral filtering. This indicates the trade-off between the spectral purity and the heralding efficiency of the silicon waveguide HSPSs; for example, increasing the purity from 77% to 92%, by increasing r from 1 to 2, approximately halves the heralding efficiency. Our heralding efficiency is mainly limited by the 28.18% waveguide-to-fiber collection efficiency (-5.5 dB loss) and the extra loss (-8.4 dB) in our waveguide structure. For the design parameters of the waveguides, based on Refs. [36,45–47], see the Supplemental Material [41].

Figure 1(e) shows that the measured heralded $g_H^{(2)}(0)$, representing the photon-number purity, decreases with increasing pump power due to the multipair contribution. This graph is useful to estimate the number purity for a required pump power (i.e., brightness), which drastically affects the indistinguishability measurements [Fig. 2(d)]. Experimentally, $g_H^{(2)}(0)$ is estimated using the following:

$$g_H^{(2)}(0) = \frac{D_3 D_{312}}{D_{31} D_{32}}, \qquad (14)$$

where D_{312} is the threefold coincidence and D_{31} and D_{32} are twofold coincidences. The fitting of the $g_H^{(2)}(0)$ data is a sigmoidal function based on Ref. [48] (for the fitting equation, see the Supplemental Material [41]).

We note that unheralded $g^{(2)}(0)$ measurements are not free from drawbacks. Since it does not involve both the signal and the idler photons, the advantage of uncorrelated noise reduction in the time-correlated measurements of photon pairs cannot be employed [35]. The noise can originate either on the chip or outside the chip—in the optical fibers, the filters, and the erbium-doped fiber amplifier (EDFA). The noise outside the chip is accounted for by bypassing the chip and it does not change the measurements appreciably. The main source of noise originates on the chip, where pump scattering is the primary contributor
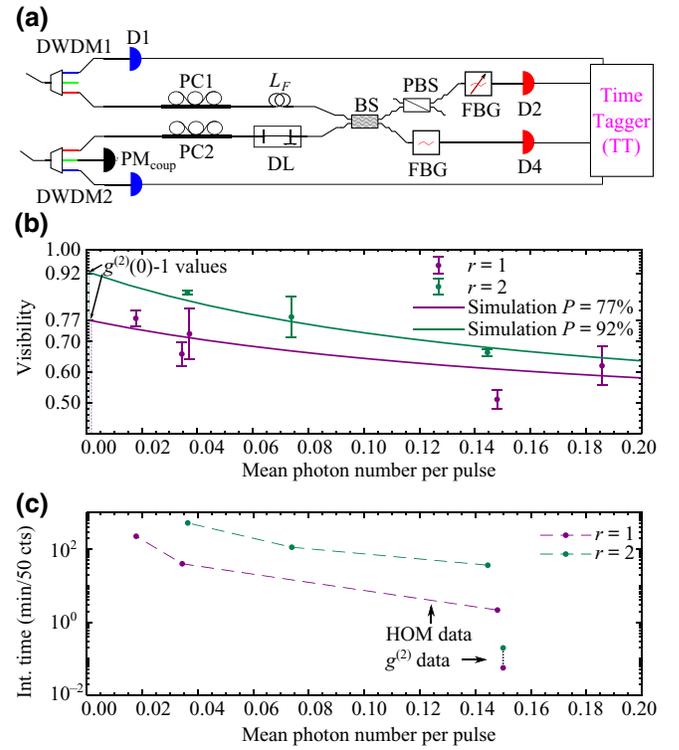

FIG. 2. The off-chip HOM interferometer: (a) the experimental setup; (b) the visibility as a function of the spectral and photon-number purity. (c) The measurement time increases exponentially to achieve higher raw indistinguishability. L_F: the length of the fibre delay line; PBS: polarisation beam splitter; FBG: fibre Bragg gratings.

[49]. Other linear and nonlinear scattering (e.g., Raman) [50] and spurious SFWM in the chip may also affect the result. A thorough characterization of these noises to correct $g^{(2)}(0)$ is beyond the scope of this experiment. The dead time of the electronics of the time-tagger can also bias the photon counting [51], which is avoided by keeping the count rates below the megacounts-per-second range.

IV. INDISTINGUISHABILITY (HOM INTERFERENCE) MEASUREMENTS

The two waveguides on the same chip are used as two independent HSPSs and are interfered on an off-chip HOM configuration to investigate the indistinguishability. Due to the long duration of a four-photon experiment, not all of the data points in Fig. 1(d) can be verified by HOM interference measurements. We choose two filter ratios, $r = 1$ and $r = 2$, to investigate the effect of spectral purity on the indistinguishability. For each of the filter ratios, three different pump powers are used to perform HOM interferences to investigate the effect of photon-number purity.

Figure 2(a) shows the experimental setup after the light is coupled out of the two waveguides. The two DWDMs separate the signal and idler photons. The idler photons

are detected (D1, D3) and herald the presence of two signal photons. One of the signal photons goes straight to the 50:50 beam splitter (BS) and the other first goes through a variable optical-delay line and then to the BS. The delay line is used to vary the arrival time of the photon's wave packet interfering on the beam splitter. A polarization beam splitter (PBS) after the BS and polarization controllers before the BS are used to ensure the same polarization of the photons interfering in the BS. After the interference in the BS, the photons are spectrally filtered by fiber Bragg gratings (FBGs) to implement $r = 2$. In the absence of FBGs, $r = 1$ is implemented as the line width of the DWDMs matches the pump line width.

Figure 2(b) depicts the effect of spectral and photon-number impurity on the indistinguishability, measured by HOM visibility (for the HOM interferograms, see the Supplemental Material [41]). The magenta ($r = 1$) and green ($r = 2$) dots are the measured data points and the solid lines are the analytical (and numerical) estimations of the visibility as a function of both of the purities. The data and the simulation show the trend that the visibility improves with a lower mean photon-number per pulse ($\bar{n}$) and narrower (e.g., $r = 2$) filtering. As $\bar{n}$ decreases, the photon-number purity keeps increasing [measured in Fig. 1(e)] until it reaches $\bar{n} \approx 0$ (the y intercept), where it is approximately unity. At the y intercept, the value of the visibility (V) is not unity but is equal to the spectral purity (P) estimated from the $g^{(2)}(0)$ measurements.

The significance of the y intercept of Fig. 2(b) can also be noted by making a connection with Fig. 1. The JSA simulations that are used to match the $g^{(2)}(0)$ measurements in Fig. 1(d) also give the strengths of the Schmidt-mode coefficients [Eq. (7); see also Fig. S3 in the Supplemental Material [41]]. These coefficients are used in our analytical model [Eq. (12) or numerical simulator] with higher-order photon-number states to calculate the visibility as a function of the mean photon number in Fig. 2(b). Since, at the y intercept of the graph, the higher-order photon-number states are practically nonexistent, the visibility depends almost entirely on the spectral purity, provided that the other contributing factors to distinguishability, such as spatial-mode mismatch, are negligible, which holds true in integrated-waveguide photonics. Both our analytical and numerical models give values of y intercepts that match well with the spectral-purity value estimated from the unheralded $g^{(2)}(0)$ measurements, thereby confirming that $V = P$ when the photon-number purity is unity and that spectral and photon-number impurity are the two main factors degrading indistinguishability in integrated-waveguide photonics.

Figure 2(c) depicts the exponential rise of the integration time of the HOM measurements when a narrower filter and a lower power are used to improve the purities. Here, the HOM measurement time is the collection time of two fourfold coincidence data points—the theoretical

minimum required to estimate HOM visibility, although in practice more points are desired. This plot shows a clear advantage of $g^{(2)}(0)$ as a faster measurement compared to HOM measurements. For example, the time required to achieve the fastest HOM-visibility data point [Fig. 2(b)] with 6% uncertainty is more than 35 times slower than the corresponding $g^{(2)}(0)$ data with the same uncertainty.

Also, a comparison between Figs. 1(a) and 2(a) shows the simplicity and robustness of the $g^{(2)}(0)$-measurement setup. The two $g^{(2)}(0)$ measurements and the heralding efficiency have the same setup, consisting of a beam splitter, a time tagger, and a delay (τ) implemented electronically. In contrast, the HOM interferometer additionally requires delay lines, a polarization controller, and a polarization beam splitter, with careful estimations of path-length differences and alignment, and the need to ensure the same polarization of the photons. The $g^{(2)}(0)$ measurements are robust since the outcome is not affected by either the detection efficiency or the splitting ratio of the beam splitter [52], which is why $g^{(2)}$ was one of the earlier demonstrations of the nonclassicality of light [27,53]. Therefore, the $g^{(2)}(0)$ measurements together with the simulations in Fig. 2(b) efficiently estimate the indistinguishability of an HSPS.

V. CONCLUSION

The strip waveguide is one of the simplest structure in silicon photonics. The modeling and understanding of the dynamics of photon-pair generation in a strip waveguide will lead the way to high-fidelity quantum technologies and potential applications in simulation and sensing with other emerging fields such as biotechnology.

For large-scale quantum information processing, we need to build multiplexed sources that will act as near-ideal single-photon sources. Considering the simplicity and stability of strip-waveguide sources among silicon-photonic structures, they provide a reasonable candidate for the development of near-ideal SPSs. However, getting around the inevitably low heralding efficiency will require sophisticated multiplexing schemes, leading to large footprints.

Indistinguishability measurements of the HSPSs using a HOM interferometer are a direct way of estimating the quality of the single photons and the scalability of the source for multiplexing and often essential to gauge the performance of a quantum-photonic protocol. However, heralded-HOM experiments involve four-photon detections, which can lead to extremely low count rates and long experimental durations. In fact, as the photonic circuit grows larger to implement the more complex quantum algorithm and thus multiple HSPSs are integrated, the pairwise indistinguishability measurements among the HSPSs become exponentially

demanding. Here, we show that capturing photon statistics with relatively quick $g^{(2)}(0)$ measurements gives a good estimate of indistinguishability, which is useful during the rapid prototyping phase of silicon-photonic source design. These measurements also estimate the heralding efficiency, which determines the integration time of the experiment. Altogether, these results can be used as a guide to choose the appropriate filtering and input pump power to achieve the required indistinguishability within a specified time constraint for a required quantum-photonic experiment.

ACKNOWLEDGMENTS

[1] C. K. Hong, Z. Y. Ou, and L. Mandel, Measurement of Subpicosecond Time Intervals Between Two Photons by Interference, Phys. Rev. Lett. **59,** 2044 (1987).

[2] E. Knill, R. Laflamme, and G. J. Milburn, A scheme for efficient quantum computation with linear optics, Nature **409,** 46 (2001).

[3] Robert Raussendorf and Hans J. Briegel, A One-Way Quantum Computer, Phys. Rev. Lett. **86,** 5188 (2001).

[4] Daniel Gottesman and Isaac L. Chuang, Demonstrating the viability of universal quantum computation using teleportation and single-qubit operations, Nature **402,** 390 (1999).

[5] Jeremy L. O'Brien, Optical quantum computing, Science **318,** 1567 (2007).

[6] Mercedes Gimeno-Segovia, Pete Shadbolt, Dan E. Browne, and Terry Rudolph, From Three-Photon Greenberger-Horne-Zeilinger States to Ballistic Universal Quantum Computation, Phys. Rev. Lett. **115,** 020502 (2015).

[7] Terry Rudolph, Why I am optimistic about the photonic route to quantum computing, APL Photonics **2,** 030901 (2017).

[8] Jianwei Wang, Stefano Paesani, Yunhong Ding, Raffaele Santagati, Paul Skrzypczyk, Alexia Salavrakos, Jordi Tura, Remigiusz Augusiak, Laura Mančinska, Davide Bacco, Damien Bonneau, Joshua W. Silverstone, Qihuang Gong, Antonio Acín, Karsten Rottwitt, Leif K. Oxenløwe, Jeremy L. O'Brien, Anthony Laing, and Mark G. Thompson, Multidimensional quantum entanglement with large-scale integrated optics, Science **360,** 285 (2018).

[9] Xiaogang Qiang, Xiaoqi Zhou, Jianwei Wang, Callum M. Wilkes, Thomas Loke, Sean O'Gara, Laurent Kling, Graham D. Marshall, Raffaele Santagati, Timothy C. Ralph, Jingbo B. Wang, Jeremy L. O'Brien, Mark G. Thompson, and Jonathan C. F. Matthews, Large-scale silicon quantum photonics implementing arbitrary two-qubit processing, Nat. Photonics **12,** 534 (2018).

[10] H. Wang, Y. He, Y.-H. Li, Z.-E. Su, B. Li, H.-L. Huang, Xi. Ding, M.-C. Chen, C. Liu, J. Qin, J.-P. Li, Y.-M. He, C. Schneider, M. Kamp, C.-Z. Peng, S. Höfling, and C.-Y. Lu, High-efficiency multiphoton boson sampling, Nat. Photonics **11,** 361 (2017).

[11] J. C. Loredo, M. A. Broome, P. Hilaire, O. Gazzano, I. Sagnes, A. Lemaitre, M. P. Almeida, P. Senellart, and A. G. White, Boson Sampling with Single-Photon Fock States From a Bright Solid-State Source, Phys. Rev. Lett. **118,** 130503 (2017).

[12] Jeremy C. Adcock, Caterina Vigliar, Raffaele Santagati, Joshua W. Silverstone, and Mark G. Thompson, Programmable four-photon graph states on a silicon chip, Nat. Commun. **10,** 1 (2019).

[13] Guoliang Li, Jin Yao, Hiren Thacker, Attila Mekis, Xuezhe Zheng, Ivan Shubin, Ying Luo, Jin-Hyoung Lee, Kannan Raj, John E. Cunningham, and Ashok V. Krishnamoorthy, Ultralow-loss, high-density SOI optical waveguide routing for macrochip interconnects, Opt. Express **20,** 12035 (2012).

[14] Stefan Abel *et al.*, Large pockels effect in micro- and nanostructured barium titanate integrated on silicon, Nat. Mater. **18,** 42 (2019).

[15] Chen Sun *et al.*, Single-chip microprocessor that communicates directly using light, Nature **528,** 534 (2015).

[16] Anthony Laing, Alberto Peruzzo, Alberto Politi, Maria Rodas Verde, Matthaeus Halder, Timothy C. Ralph, Mark G. Thompson, and Jeremy L. O'Brien, High-fidelity operation of quantum photonic circuits, Appl. Phys. Lett. **97,** 211109 (2010).

[17] Imad I. Faruque, Gary F. Sinclair, Damien Bonneau, John G. Rarity, and Mark G. Thompson, On-chip quantum interference with heralded photons from two independent micro-ring resonator sources in silicon photonics, Opt. Express **26,** 20379 (2018).

[18] Francesco Graffitti, Peter Barrow, Massimiliano Proietti, Dmytro Kundys, and Alessandro Fedrizzi, Independent high-purity photons created in domain-engineered crystals, Optica **5,** 514 (2018).

[19] Jérémie Fulconis, Olivier Alibart, Jeremy L. O'Brien, William J. Wadsworth, and John G. Rarity, Nonclassical Interference and Entanglement Generation Using a Photonic Crystal Fiber Pair Photon Source, Phys. Rev. Lett. **99,** 120501 (2007).

[20] Z. Vernon, M. Menotti, C. C. Tison, J. A. Steidle, M. L. Fanto, P. M. Thomas, S. F. Preble, A. M. Smith, P. M. Alsing, M. Liscidini, and J. E. Sipe, Truly unentangled photon pairs without spectral filtering, Opt. Lett. **42,** 3638 (2017).

[21] Nobuyuki Matsuda and Hiroki Takesue, Generation and manipulation of entangled photons on silicon chips, Nanophotonics **5,** 440 (2016).

[22] Daniel R. Blay, M. J. Steel, and L. G. Helt, Effects of filtering on the purity of heralded single photons from parametric sources, Phys. Rev. A **96,** 053842 (2017).

[23] Evan Scott, Nicola Montaut, Johannes Tiedau, Linda Sansoni, Harald Herrmann, Tim J. Bartley, and Christine Silberhorn, Limits on the heralding efficiencies and spectral purities of spectrally filtered single photons from photon-pair sources, Phys. Rev. A **95,** 061803(R) (2017).

[24] J. Fulconis, O. Alibart, W. J. Wadsworth, and J. G. Rarity, Quantum interference with photon pairs using two micro-structured fibres, New J. Phys. **9**, 276 (2007).

[25] Ken-ichi Harada, Hiroki Takesue, Hiroshi Fukuda, Tai Tsuchizawa, Toshifumi Watanabe, Koji Yamada, Yasuhiro Tokura, and Sei-ichi Itabashi, Indistinguishable photon pair generation using two independent silicon wire waveguides, New J. Phys. **13**, 065005 (2011).

[26] W. P. Grice, A. B. U'Ren, and I. A. Walmsley, Eliminating frequency and space-time correlations in multiphoton states, Phys. Rev. A **64**, 063815 (2001).

[27] R. Hanbury Brown and R. Q. Twiss, A test of a new type of stellar interferometer on Sirius, Nature **178**, 1046 (1956).

[28] P. R. Tapster and J. G. Rarity, Photon statistics of pulsed parametric light, J. Mod. Opt. **45**, 595 (1998).

[29] Andreas Christ, Kaisa Laiho, Andreas Eckstein, Katiúscia N. Cassemiro, and Christine Silberhorn, Probing multimode squeezing with correlation functions, New J. Phys. **13**, 033027 (2011).

[30] Georg Harder, Vahid Ansari, Benjamin Brecht, Thomas Dirmeier, Christoph Marquardt, and Christine Silberhorn, An optimized photon pair source for quantum circuits, Opt. Express **21**, 13975 (2013).

[31] N. Bruno, A. Martin, T. Guerreiro, B. Sanguinetti, and R. T. Thew, Pulsed source of spectrally uncorrelated and indistinguishable photons at telecom wavelengths, Opt. Express **22**, 17246 (2014).

[32] Liang Cui, Xiaoying Li, and Ningbo Zhao, Minimizing the frequency correlation of photon pairs in photonic crystal fibers, New J. Phys. **14**, 123001 (2012).

[33] C. Clausen, F. Bussières, A. Tiranov, H. Herrmann, C. Silberhorn, W. Sohler, M. Afzelius, and N. Gisin, A source of polarization-entangled photon pairs interfacing quantum memories with telecom photons, New J. Phys. **16**, 093058 (2014).

[34] Stefano Paesani, Yunhong Ding, Raffaele Santagati, Levon Chakhmakhchyan, Caterina Vigliar, Karsten Rottwitt, Leif K. Oxenløwe, Jianwei Wang, Mark G. Thompson, and Anthony Laing, Generation and sampling of quantum states of light in a silicon chip, Nat. Phys. **15**, 925 (2019).

[35] Andreas Eckstein, Andreas Christ, Peter J. Mosley, and Christine Silberhorn, Realistic $g^{(2)}$ measurement of a PDC source with single photon detectors in the presence of background, Phys. Status Solidi C **8**, 1216 (2011).

[36] Robert W. Boyd, *Nonlinear Optics* (Elsevier, New York, 2008), p. 605.

[37] Christopher C. Gerry and Peter L. Knight, *Introductory Quantum Optics* (Cambridge University Press, 2005).

[38] Andreas Eckstein, Guillaume Boucher, Aristide Lemaître, Pascal Filloux, Ivan Favero, Giuseppe Leo, John E. Sipe, Marco Liscidini, and Sara Ducci, Bi-photon spectral correlation measurements from a silicon nanowire in the quantum and classical regimes, Laser Photon. Rev. **8**, L76 (2014).

[39] Iman Jizan, L. G. Helt, Chunle Xiong, Matthew J. Collins, Duk-Yong Choi, Chang Joon Chae, Marco Liscidini, M. J. Steel, Benjamin J. Eggleton, and Alex S. Clark, Bi-photon spectral correlation measurements from a silicon nanowire in the quantum and classical regimes, Sci. Rep. **5**, 12557 (2015).

[40] Iman Jizan, Bryn Bell, L. G. Helt, Alvaro Casas Bedoya, Chunle Xiong, and Benjamin J. Eggleton, Phase-sensitive tomography of the joint spectral amplitude of photon pair sources, Opt. Lett. **41**, 4803 (2016).

[41] See the Supplemental Material at http://link.aps.org/supplemental/10.1103/PhysRevApplied.12.054029 for detailed data analysis and the derivations of the equations presented in this paper.

[42] Wolfgang Mauerer, Malte Avenhaus, Wolfram Helwig, and Christine Silberhorn, How colors influence numbers: Photon statistics of parametric down-conversion, Phys. Rev. A **80**, 053815 (2009).

[43] X. Zhang, R. Jiang, B. Bell, D.-Y. Choi, C. Chae, and C. Xiong, Interfering heralded single photons from two separate silicon nanowires pumped at different wavelengths, Technologies **4**, 25 (2016).

[44] I. I. Faruque, G. F. Sinclair, D. Bonneau, T. Ono, C. Silberhorn, M. G. Thompson, and J. G. Rarity, Data for: "Estimating indistinguishability of heralded single-photons using second-order correlation," https://doi.org/10.5523/bris.2779vw6bml4cj2e5t3u9584fpf (2019).

[45] Damien Bonneau, Joshua W. Silverstone, and Mark G. Thompson, *Silicon Quantum Photonics III*. Topics in Applied Physics (Springer publication, Heidelberg, Germany) Vol. 122 (2016).

[46] Gary F. Sinclair and Mark G. Thompson, Effect of self- and cross-phase modulation on photon pairs generated by spontaneous four-wave mixing in integrated optical waveguides, Phys. Rev. A **94**, 063855 (2016).

[47] Lukas G. Helt, Marco Liscidini, and John E. Sipe, How does it scale? Comparing quantum and classical nonlinear optical processes in integrated devices, J. Opt. Soc. Am. B **29**, 2199 (2012).

[48] Chaoxuan Ma, Xiaoxi Wang, Vikas Anant, Andrew D. Beyer, Matthew D. Shaw, and Shayan Mookherjea, Silicon photonic entangled photon-pair and heralded single photon generation with CAR > 12, 000 and $g^{(2)}(0) < 0006$, Opt. Express **25**, 32995 (2017).

[49] Mateusz Piekarek, Damien Bonneau, Shigehito Miki, Taro Yamashita, Mikio Fujiwara, Masahide Sasaki, Hirotaka Terai, Michael G. Tanner, Chandra M. Natarajan, Robert H. Hadfield, Jeremy L. O'Brien, and Mark G. Thompson, High-extinction ratio integrated photonic filters for silicon quantum photonics, Opt. Lett. **42**, 815 (2017).

[50] Cale M. Gentry, Omar S. Magaña-Loaiza, Mark T. Wade, Fabio Pavanello, Thomas Gerrits, Sen Lin, Jeffrey M. Shainline, Shellee D. Dyer, Sae Woo Nam, Richard P. Mirin, and Miloš A. Popović, in *Conference on Lasers and Electro-Optics* (OSA, San Jose, 2018), p. JTh4C.3.

[51] M. Beck, Comparing measurements of $g^{(2)}(0)$ performed with different coincidence detection techniques, J. Opt. Soc. Am. B **24**, 2972 (2007).

[52] Rodney Loudon, *The Quantum Theory of Light* (Oxford University Press, 2000), 3rd ed.; Leonard Mandel and Emil Wolf, *Optical Coherence and Quantum Optics* (Cambridge University Press, 1995).

[53] H. J. Kimble, M. Dagenais, and L. Mandel, Photon Antibunching in Resonance Fluorescenc, Phys. Rev. Lett. **39**, 691 (1977).